Mixed Zn and O substitution of Co and Mn in ZnO

L. M. C. Pereira,[1,2,3,*] U. Wahl,[2,4] S. Decoster,[1] J. G. Correia,[2,4] L. M. Amorim,[1] M. R. da Silva,[4]
J. P. Araújo,[3] and A. Vantomme[1]

[1]*Instituut voor Kern- en Stralingsfysica and INPAC, K.U. Leuven, B-3001 Leuven, Belgium*
[2]*Instituto Tecnológico e Nuclear, UFA, P-2686-953 Sacavém, Portugal*
[3]*IFIMUP and IN–Institute of Nanoscience and Nanotechnology, Department of Physics and Astronomy,
Faculdade de Ciências da Universidade do Porto, P-4169-007 Porto, Portugal*
[4]*Centro de Física Nuclear da Universidade de Lisboa, P-1649-003 Lisboa, Portugal*

The physical properties of an impurity atom in a semiconductor are primarily determined by the lattice site it occupies. In general, this occupancy can be correctly predicted based on chemical intuition, but not always. We report on one such exception in the dilute magnetic semiconductors Co- and Mn-doped ZnO, experimentally determining the lattice location of Co and Mn using β^--emission channeling from the decay of radioactive ^{61}Co and ^{56}Mn implanted at the ISOLDE facility at CERN. Surprisingly, in addition to the majority substituting for Zn, we find up to 18% (27%) of the Co (Mn) atoms in O sites, which is virtually unaffected by thermal annealing up to 900 °C. We discuss how this anion site configuration, which had never been considered before for any transition metal in any metal oxide material, may in fact have a low formation energy. This suggests a change in paradigm regarding transition-metal incorporation in ZnO and possibly other oxides and wide-gap semiconductors.

I. INTRODUCTION

Among the many combinations of host materials and transition-metal dopants investigated in the past two decades, Co- and Mn-doped ZnO are currently two of the most intensively studied dilute magnetic semiconductors (DMSs). However, despite major developments in both synthesis and characterization methods, the magnetism of wide-gap semiconductors remains one of the most controversial topics in condensed-matter physics.[1]

Key to the understanding of DMS materials is the local structure of the transition-metal (TM) atoms in the host semiconductor matrix. The occupied lattice site determines the electronic structure of the impurity atom and, consequently, its electrical and magnetic character. Intrinsic point defects, e.g., vacancies and self-interstitials, may form complexes with an impurity atom and change its charge state and magnetic moment or even mediate magnetic interactions. Another crucial parameter in DMS materials, the impurity spatial distribution (dilution versus aggregation), depends on the diffusivity of the impurity atoms, which in turn is controlled by the thermal stability of their local structure configuration(s). Stemming from a growing awareness of this complex influence on the magnetic properties, the lattice location of 3d transition metals in ZnO has been extensively studied in the last few years, mostly based on x-ray absorption fine structure techniques (e.g., Refs. 2–4 for Co and Refs. 5–7 for Mn), incorporated either during growth[2–6,8] or by ion implantation.[7,9] When secondary phase segregation is avoided, all 3d TMs, including Co and Mn, were always found to substitute Zn, independently of the growth method,[10] as expected from the chemical similarities between the impurities and the host elements. The Zn substitution by Co^{2+} impurities has also been inferred from electron paramagnetic resonance experiments (e.g., Refs. 11 and 12 and references therein) and confirmed by x-ray linear dichroism measurements.[13] However, some observations do not completely conform to the scenario where all impurities occupy Zn substitutional sites in ZnO. X-ray absorption near-edge structure spectroscopy[4,14] and x-ray photoelectron spectroscopy[15] experiments have shown that Mn impurities can be incorporated in ZnO with charge states of up to 4+. Because Zn-substitutional Mn is expected to have a 2+ charge state with the 2+/3+ and 3+/4+ donor levels below the valence band maximum (thus not ionized),[16] these reports indicate that minority fractions may in fact occupy other lattice sites.

Here we report on the lattice location of ion-implanted Co and Mn in ZnO, in the as-implanted state and after thermal annealing up to 900 °C, using the emission channeling (EC) technique.

II. EXPERIMENT

Emission channeling[17] makes use of the charged particles emitted by a radioactive isotope. The screened Coulomb potential of atomic rows and planes determines the anisotropic scattering of the particles emitted isotropically during decay. Since these channeling and blocking effects strongly depend on the initial position of the emitted particles, they result in emission patterns that are characteristic of the lattice site(s) occupied by the probe atoms. The EC technique is ideal to study the lattice location of transition metals in semiconductors, as we have shown, for example, for Fe (Ref. 18), Cu (Ref. 19), and Ag (Ref. 20) in ZnO. It is particularly suited for those cases where significant fractions of the transition-metal atoms occupy more than one lattice site (e.g., Ref. 21). For Mn impurities specifically, this multisite lattice location capability has recently allowed us to locate a fraction of implanted Mn on the bond-centered (BC) site in Ge (Ref. 22) and to unambiguously identify the interstitial Mn site in GaAs and quantitatively study its thermal stability.[23]

Commercially available ZnO wurtzite [0001] single crystals (CrysTec GmbH), hydrothermally grown and Zn-face polished, were implanted at room temperature at the online

isotope separator facility ISOLDE at CERN. As a Mn probe, we implanted radioactive ^{56}Mn ($t_{1/2} = 2.56$ h) and measured the β^- particles emitted during the decay to stable ^{56}Fe. For Co, we implanted the precursor isotope ^{61}Mn with the decay chain ^{61}Mn (0.71 s) $\rightarrow$ ^{61}Fe (6 min) $\rightarrow$ ^{61}Co (1.6 h) $\rightarrow$ ^{61}Ni (stable). In order to ensure that the contributions of ^{61}Mn and ^{61}Fe β^- particles to the channeling patterns were negligible, the measurements started only after a waiting period of approximately 30–60 min. The β^- decay of ^{61}Fe transfers a recoil energy of about 103 eV to its ^{61}Co daughter. This is well above the threshold displacement energy of ZnO (57 eV)[24] and is therefore sufficiently high to reimplant the ^{61}Co atoms, ensuring that they do not inherit the ^{61}Fe lattice site. The ^{61}Mn (^{56}Mn) implantations were performed under a tilt angle of 17° with respect to the surface normal in order to minimize ion channeling, with an energy of 60 keV (50 keV) and a fluence of 2×10^{13} cm^{-2}, resulting in a peak concentration of 6×10^{18} cm^{-3} (7×10^{18} cm^{-3}) at a projected range R_p of 278 Å (246 Å) with a 125 Å (115 Å) straggling, estimated using the MARLOWE code.[25] The low-concentration regime used in this study (below 1×10^{19} cm^{-3}) allows us to investigate the lattice location of Co and Mn free from phase segregation, which typically occurs for concentrations of the order of 1×10^{21} cm^{-3} (i.e., three orders of magnitude higher) and above.[26]

Angular-dependent emission yields of the β^- particles emitted during decay were measured at room temperature, along four crystallographic directions, [0001], [$\underline{1}$102], [$\underline{1}$101] and [$\underline{2}$113], in the as-implanted state and after *in situ* capless annealing in vacuum ($<10^{-5}$ mbar) at temperatures up to 900°C. These patterns were recorded using a position- and energy-sensitive detection system similar to that described in Ref. 27. Given the relatively short half-life of ^{56}Mn and ^{61}Co, this system was installed online and upgraded with self-triggering readout chips for the Si pad detectors, enabling measurements during and/or immediately after implantation with count rates of up to several kilohertz.

III. RESULTS AND DISCUSSION

The quantitative lattice location is provided by fitting the experimental patterns with theoretical ones using the two-dimensional fit procedure outlined in Ref. 27. The theoretical patterns were calculated using the *many-beam* formalism[17] for probes occupying various sites in the ZnO (wurtzite) structure described in Ref. 28: substitutional Zn (S_{Zn}) and O (S_O) sites with varying rms displacements, the main interstitial sites, i.e., tetrahedral (T), octahedral (O), hexagonal (H), BC, and antibonding (AB), as well as interstitial sites resulting from displacements along the c or the basal directions. For all four measured directions in both ^{61}Co:ZnO and ^{56}Mn:ZnO, the calculated S_{Zn} patterns gave by far the best agreement, showing that the majority of the probe atoms occupy S_{Zn} sites, as expected. The fitting routine was then allowed to include, in addition to S_{Zn}, an additional lattice site, for which all the simulated sites were tested. The $S_{Zn} + S_O$ double occupancy gives the best fit compared to all other combinations and considerably improves the S_{Zn} single-site fit. This is illustrated in Fig. 1, which shows the reduced χ^2 of the fit as we *move* the non-S_{Zn} site along the c axis between two neighboring

S_{Zn} sites. Data are shown only for the off-surface directions [$\underline{1}$102], [$\underline{1}$101], and [$\underline{2}$113], since the [0001] patterns are not sensitive to displacements of the probe atoms along the c axis. Consistently for all three directions, the best fits are clearly centered on the S_O site. In fact, the relative improvement in χ^2 is correlated with the spatial separation of Zn and O rows along the channeling axis (Fig. 1), being most pronounced for the [$\underline{2}$113] direction. A similar behavior is observed for displacements along the basal directions, with the best fit consistently centered on the S_O site. As an example for the good match between experiment and simulated patterns, Fig. 2 compares the β^--emission yields of ^{61}Co:ZnO along the four measured directions with the best fits of theoretical patterns, obtained for 82% of the ^{61}Co atoms on S_{Zn} (Co$_{Zn}$) and 18% on S_O sites (Co$_O$). Introducing a third site yields only insignificant fit improvements. Possible fractions on other sites are estimated to be below 5%.

In Fig. 3 we have compiled the Co and Mn fractions on S_{Zn} and S_O sites as a function of annealing temperature. Within experimental error, both the Co$_O$ and Mn$_O$ fractions remain constant around 16% and 24%, respectively, up to the highest temperature annealing step. The best fits are obtained for rms displacements of Co$_{Zn}$ and Mn$_{Zn}$ from ideal S_{Zn} sites between 0.06 and 0.09 Å. Although the fitting is less sensitive to rms displacements of the Co$_O$ and Mn$_O$ minority fractions, it indicates that these may be isotropically scattered by up to
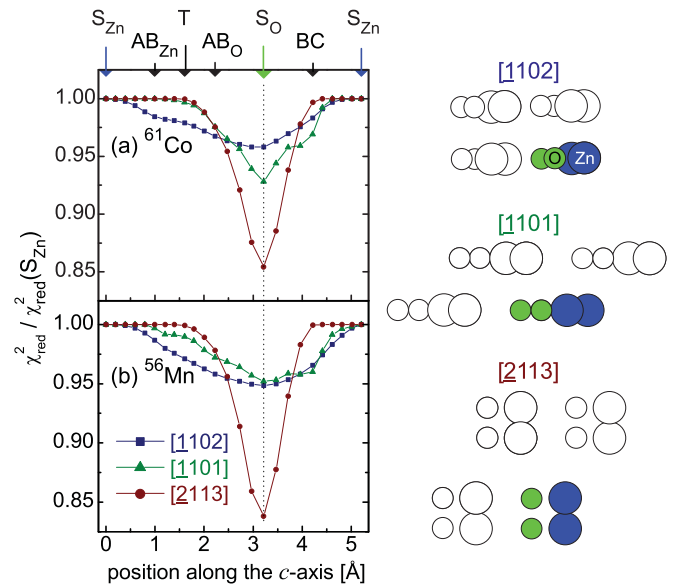
FIG. 1. (Color online) (left) Reduced χ^2 of the fits to the (a) ^{61}Co:ZnO and (b) ^{56}Mn:ZnO data (800°C annealing step), in the vicinity of the [$\underline{1}$102], [$\underline{1}$101], and [$\underline{2}$113] directions. Each data point corresponds to the best fit obtained using two given sites, with the corresponding two fractions as free parameters. The site pairs are composed of S_{Zn} plus each of the simulated sites along the c axis: the S_O and the T sites, the BC and AB sites along the c axis, and a number of intermediate positions. The reduced χ^2 (y axis) of these two-site fits have been normalized to that of the one-site (S_{Zn}) fit. The x axis corresponds to the position (along the c axis) of the non-S_{Zn} site used in each fit. (right) Projection of the ZnO lattice on the plane perpendicular to each direction, showing that the separation between Zn and O sublattices is maximized for [$\underline{2}$113].
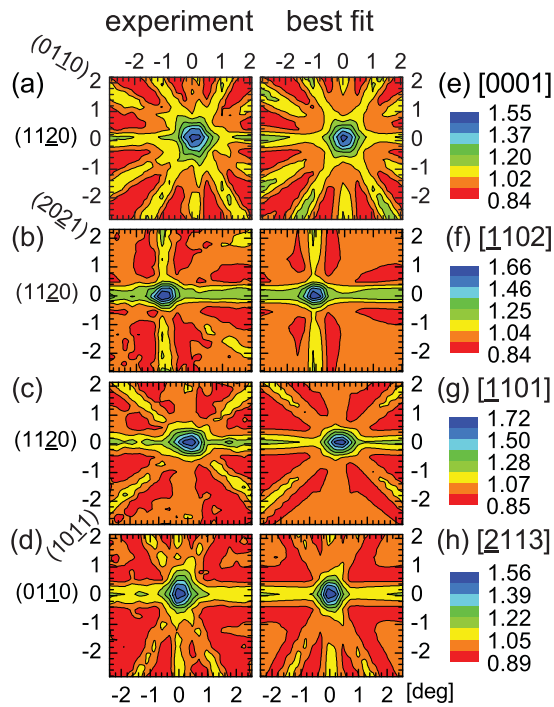
FIG. 2. (Color online) (a–d) Normalized experimental ^{61}Co β^--emission channeling patterns in the vicinity of the [0001], [$\underline{1}$102], [$\underline{1}$101], and [$\underline{2}$113] directions following annealing at 800 °C. (e–h) Corresponding best fits with 82% and 18% of the ^{61}Co atoms on S_{Zn} and S_O sites, respectively.

0.25 Å around the ideal O sites. Based on the thermal vibration amplitudes of $u_1(Zn) = 0.08$ Å and $u_1(O) = 0.08$–0.09 Å for Zn and O, respectively,[29] we conclude that, while Co_{Zn} and Mn_{Zn} atoms are incorporated in ideal Zn sites, some degree of lattice relaxation may take place in the vicinity of Co_O and Mn_O atoms.

It is interesting to compare this behavior to that of Fe, which is positioned between Co and Mn in the periodic system. In our previous EC experiments on ^{59}Fe:ZnO, the maximum fraction of Fe on substitutional O sites compatible with the experimental data is less than 5%, which is considered below the sensitivity limit of the technique.[18] The average β^- energies for ^{61}Co and ^{56}Mn are 460 and 831 keV, respectively,
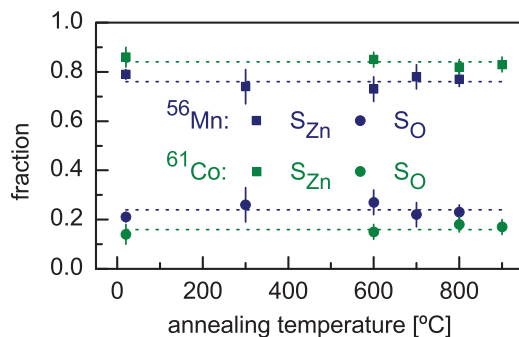
FIG. 3. (Color online) Fractions of ^{56}Mn and ^{61}Co atoms on S_{Zn} and S_O sites following each annealing step. The dashed lines correspond to the mean fractions, averaged from the values for the different annealing steps.

and are thus significantly larger than the one for ^{59}Fe, which is 118 keV. Since a higher β^- energy results in narrower channeling effects, the experimental patterns from ^{61}Co and ^{56}Mn are less resolved than those previously measured for ^{59}Fe. In order to exclude that this would influence the analysis, we carried out a ^{56}Mn:ZnO EC experiment with increased angular resolution. To do so, we doubled the distance between the sample and the detector (from 30 to 60 cm), thus improving the angular resolution by approximately a factor of 2. The analysis of these high-resolution data confirms the S_O occupancy and, in fact, the experimental patterns even allow for its visual identification. This is illustrated in Fig. 4, which compares calculated patterns for ^{56}Mn probes on S_{Zn} and S_O to experimental patterns from which the S_{Zn} component has been subtracted. The S_{Zn}-subtracted patterns are remarkably similar to S_O and very different from S_{Zn} patterns, which unambiguously confirms the S_O occupancy. Looking for other potential spurious origins for the fitted S_O fraction, one might consider secondary phases. However, secondary phase formation is extremely unlikely in our samples, as the very low Co and Mn concentrations make it nearly impossible that such large fractions (about 16% and 24% of Co and Mn, respectively) diffuse and segregate at room temperature. For Co, for example, such high fractions (17%) of segregated impurities are only observed at concentrations three orders of magnitude higher,[26] even for implantation temperatures of 350 °C at which the Co mobility is higher. For lower concentrations, no secondary phases can be resolved, even using synchrotron radiation x-ray diffraction,[26] which means that if a secondary phase *does* form, it is either (1) a wurtzite CoO phase which is perfectly coherent with the ZnO structure or (2) disordered or even amorphous CoO_x phases. However, for such secondary phases to emulate the observed O substitution, the Co atoms must be aligned with the O sublattice within less than 0.25 Å along all four measured crystal axes (c.f. previous paragraph). This is not the case for scenario 1, where the Co atoms would be aligned with the Zn sublattice instead. This is not the case for scenario 2 either, where the Co would be randomly distributed with respect to the measured crystal axes, thus contributing with a nearly isotropic background rather than the anisotropic patterns characteristic of S_O sites (Fig. 4).

Finding significant fractions of Co and Mn atoms on O sites is remarkably surprising. Not only has it never been observed, it has never even been considered since the Zn substitution was regarded as obvious and taken for granted. Moreover, experimentally identifying a minority site in cases of double occupancy is extremely challenging. These two factors (being unexpected and difficult to detect) could explain why such anion site minority fractions may have passed undetected in previous studies on the lattice location of Mn and Co in ZnO, incorporated either during growth (e.g., Refs. 2–6,8) or by ion implantation (e.g., Refs. 7 and 9).

Generally, in compound semiconductors, the lattice sites of impurities are determined by chemical similarities and matching of size and electronegativity with the host atoms. Not only are Co and Mn 3*d* metals like Zn, they are very similar to Zn and very different from O in terms of electronegativity and ionic radii, which in principle makes it energetically unfavorable for Co and Mn impurities to be incorporated
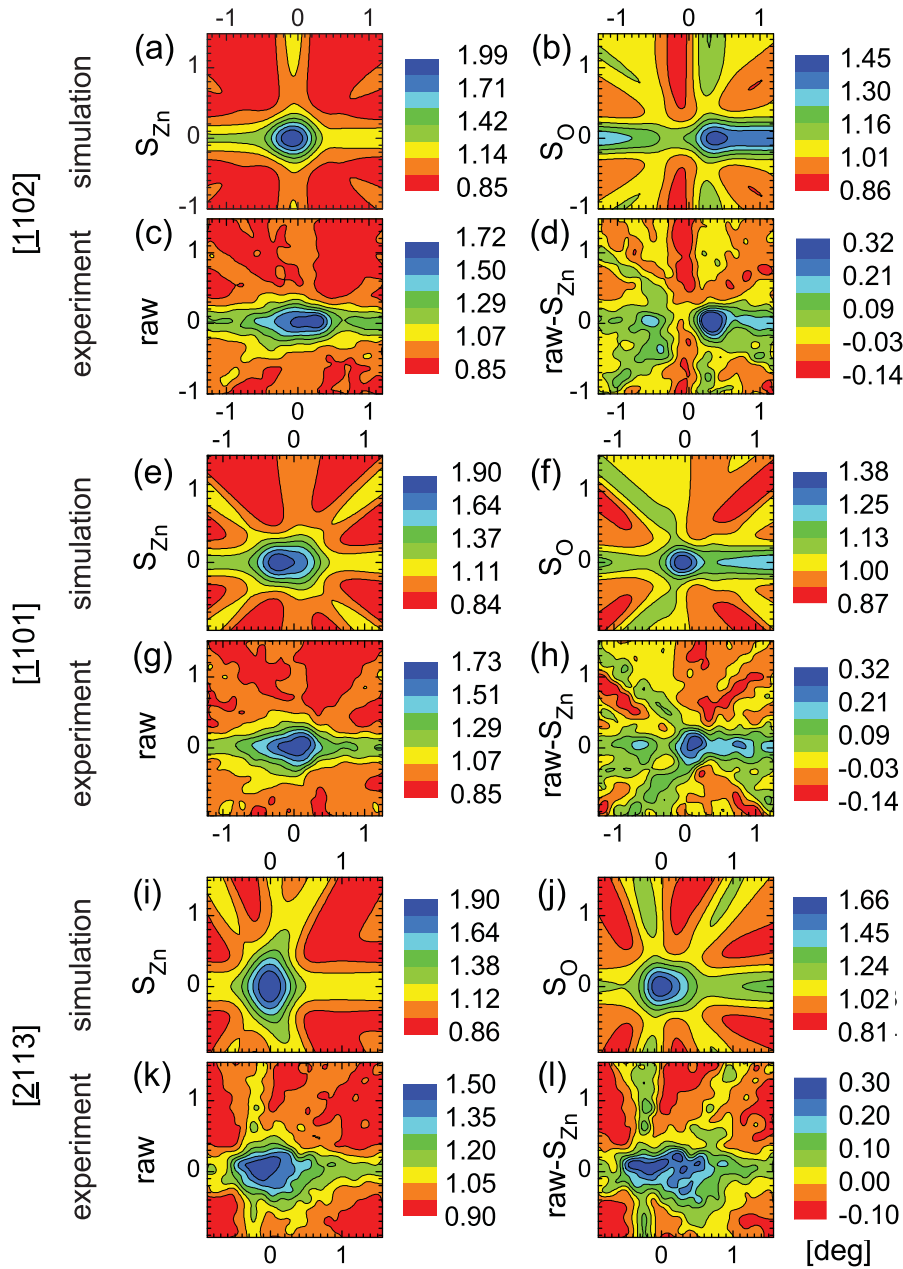
FIG. 4. (Color online) Comparison of the experimental and calculated patterns of the high-resolution, as-implanted ^{56}Mn:ZnO experiment: calculated [$\underline{1}$102], [$\underline{1}$101], and [$\underline{2}$113] patterns for 100% of ^{56}Mn probes on (a, e, i) S_{Zn} and (b, f, j) S_O sites; (c, g, k) normalized experimental patterns. (d, h, l) Patterns result from subtracting the fitted S_{Zn} component from the experimental patterns. For all three directions, this allows for the visual identification of the S_O occupancy; i.e. patterns in (d), (h), and (l) reproduce the distinctive features of the S_O patterns in (b), (f), and (j), respectively.

on O sites. The nonequilibrium nature of ion implantation may have an influence, but it does not explain why, under the same conditions, the S_O occupancy is observed for Mn and Co and not for Fe. The case that has been studied theoretically which most resembles Mn_O and Co_O defects is the Zn antisite (Zn_O). Depending on the growth conditions (Zn- or O-rich) and Fermi level, either 2^+, 3^+, or 4^+ charge states of Zn_O can be stable, with the $4^+/3^+$ and $3^+/2^+$ transition levels deep in the band gap.[30–33] These calculations predicted that the formation energy of Zn_O^{4+} can in fact be very small, even negative, under metal-rich conditions and for a Fermi level close to the valence band maximum. Therefore, if the $4^+/3^+$ and $3^+/2^+$ transition levels of Co_O and Mn_O are shallower than those of Zn_O, it is conceivable that the formation energies of Co_O and Mn_O may indeed be small enough to allow for sizable concentrations, even with the Fermi level close to the conduction band minimum, which is typically the case for

ZnO (intrinsically *n* type). On the other hand, the $4^+/3^+$ and $3^+/2^+$ levels of Fe_O may be located deeper in the band gap and therefore not be ionized when the Fermi level is close to the conduction band minimum. Based on the Zn_O case, this would result in a higher formation energy of Fe_O compared to Co_O and Mn_O and thus decrease its concentration below the detection limit.

An important consequence of the previous paragraph is that O substitution can thus explain the observed $4+$ charge state of minority fractions of Mn impurities in ZnO thin films.[4,14,15] Moreover, the fact that for those studies the impurities were incorporated not by ion implantation but during growth indicates that minority anion substitution may be a general phenomenon in transition-metal-doped ZnO. In principle, the concentration of transition-metal impurities in anion sites increases with (1) decreasing energy cost of incorporating an atom of a given impurity element in an O site and (2)

increasing available energy. The energy cost (1) depends on (i) the impurity-host combination, which for the ZnO host case appears to favor Co and Mn over Fe based on our results and the discussion of the previous paragraph, and (ii) the tendency of the growth or doping process to form O vacancies which can be filled by transition-metal impurities (for doping during growth this is favored in O-poor conditions; in ion-implanted systems O vacancies are created by the ion bombardment). The available energy (2) depends on the growth or doping method and conditions, increasing with the characteristic order of magnitude of impinging atom energies: 0.1 eV for molecular beam epitaxy, 1 eV for sputtering deposition, 10 eV for pulsed laser deposition (PLD), and 1 keV for ion implantation. One can thus expect higher anion site fractions for processes such as PLD growth in O-poor conditions and ion implantation compared to that for processes closer to equilibrium.

Because the magnetic and electric behavior of Co and Mn impurities depends primarily on the lattice site(s) they occupy, our results have direct implications on the field of dilute magnetic semiconductors. For example, anion site Mn and Co are likely to behave as multiple-donor defects in ZnO and thus contribute to preventing the realization of p-type conduction (by acceptor codoping) in TM-doped ZnO, which is considered crucial to establish ferromagnetic order via p-d Zener exchange.[34] A similar case is the well-known double-donor Mn interstitial in (Ga,Mn)As, which compensates for acceptor substitutional Mn both electrically and magnetically, thus decreasing the Curie temperature.[35] Also, in Mn-doped GaN, the presence of donor defects controls the charge state of cation (Ga) substitutional Mn and hence the type

of magnetic interactions: ferromagnetic for Mn^{3+} (Ref. [36]) antiferromagnetic for Mn^{2+} (Ref. [37]).

IV. CONCLUSIONS

In summary, we have experimentally established the lattice location of implanted Co and Mn in ZnO in the low-concentration regime ($<10^{18}$ cm^{-3}). Surprisingly, in addition to the majority of substitutional Zn sites, we find up to 18% (27%) of the Co (Mn) atoms on substitutional O sites, which is virtually unaffected by thermal annealing up to 900 °C. Because this minority anion site substitution has never even been considered, it challenges our current understanding of transition-metal incorporation in ZnO and wide-gap semiconductors in general. In particular, these results motivate a theoretical assessment of the formation energies of these defects, as well as an experimental reassessment of the lattice location of Mn and Co in wide-gap semiconductors, its dependence on preparation techniques and growth conditions, and its influence on the magnetic properties of wide-gap DMS materials.

*linomcp@fc.up.pt

[1] T. Dietl, Nat. Mater. **9**, 965 (2010).

[2] T. Shi, S. Zhu, Z. Sun, S. Wei, and W. Liu, Appl. Phys. Lett. **90**, 102108 (2007).

[3] Z. Sun, W. Yan, G. Zhang, H. Oyanagi, Z. Wu, Q. Liu, W. Wu, T. Shi, Z. Pan, P. Xu, and S. Wei, Phys. Rev. B **77**, 245208 (2008).

[4] N. R. S. Farley, K. W. Edmonds, A. A. Freeman, G. van der Laan, C. R. Staddon, D. H. Gregory, and B. L. Gallagher, New J. Phys. **10**, 055012 (2008).

[5] J.-H. Guo A. Gupta, P. Sharma, K. V. Rao, M. A. Marcus, C. L. Dong, J. M. O. Guillen, S. M. Butorin, M. Mattesini, P. A. Glans, K. E. Smith, C. L. Chang, and R. Ahuja, J. Phys. Condens. Matter **19**, 172202 (2007).

[6] H. Ofuchi, Z. W. Jin, T. Fukumura, M. Kawasaki, Y. Matsumoto, T. Hasegawa, H. Fujioka, M. Oshima, and H. Koinuma, Phys. Scr., T **115**, 614 (2005).

[7] J. A. Sans, G. Martinez-Criado, J. Susini, R. Sanz, J. Jensen, I. Minguez, M. Hernandez-Velez, A. Labrador, and P. Carpentier, J. Appl. Phys. **107**, 023507 (2010).

[8] J. C. Pivin, G. Socol, I. Mihailescu, P. Berthet, F. Singh, M. K. Patel, and L. Vincent, Thin Solid Films **517**, 916 (2008).

[9] A. P. Singh, R. Kumar, P. Thakur, N. B. Brookes, K. H. Chae, and W. K. Choi, J. Phys. Condens. Matter **21**, 185005 (2009).

[10] A. Ney, M. Opel, T. C. Kaspar, V. Ney, S. Ye, K. Ollefs, T. Kammermeier, S. Bauer, K.-W. Nielsen, S. T. B. Goennenwein,

M. H. Engelhard, S. Zhou, K. Potzger, J. Simon, W. Mader, S. M. Heald, J. C. Cezar, F. Wilhelm, A. Rogalev, R. Gross, and S. A. Chambers, New J. Phys. **12**, 013020 (2010).

[11] P. Sati, R. Hayn, R. Kuzian, S. Regnier, S. Schafer, A. Stepanov, C. Morhain, C. Deparis, M. Laugt, M. Goiran, and Z. Golacki, Phys. Rev. Lett. **96**, 017203 (2006).

[12] N. Jedrecy, H. J. von Bardeleben, Y. Zheng, and J. L. Cantin, Phys. Rev. B **69**, 041308 (2004).

[13] A. Ney, K. Ollefs, S. Ye, T. Kammermeier, V. Ney, T. C. Kaspar, S. A. Chambers, F. Wilhelm, and A. Rogalev, Phys. Rev. Lett. **100**, 157201 (2008).

[14] P. Thakur, K. H. Chae, J.-Y. Kim, M. Subramanian, R. Jayavel, and K. Asokan, Appl. Phys. Lett. **91**, 162503 (2007).

[15] H. T. Cao, Z. L. Pei, J. Gong, C. Sun, R. F. Huang, and L. S. Wen, J. Solid State Chem. **177**, 1480 (2004).

[16] T. Graf, S. T. B. Goennenwein, and M. S. Brandt, Phys. Status Solidi B **239**, 277 (2003).

[17] H. Hofsass and G. Lindner, Phys. Rep. **201**, 121 (1991).

[18] E. Rita, U. Wahl, J. G. Correia, E. Alves, and J. C. Soares, Appl. Phys. Lett. **85**, 4899 (2004).

[19] U. Wahl, E. Rita, J. G. Correia, E. Alves, and J. C. Soares, Phys. Rev. B **69**, 012102 (2004).

[20] E. Rita, U. Wahl, A. M. L. Lopes, J. P. Araujo, J. G. Correia, E. Alvesa, and J. C. Soares (ISOLDE Collaboration), Physica B **340**, 240 (2003).

[21] S. Decoster, S. Cottenier, B. De Vries, H. Emmerich, U. Wahl, J. G. Correia, and A. Vantomme, Phys. Rev. Lett. **102**, 065502 (2009).

[22] S. Decoster, S. Cottenier, U. Wahl, J. G. Correia, L. M. C. Pereira, C. Lacasta, M. R. Da Silva, and A. Vantomme, Appl. Phys. Lett. **97**, 151914 (2010).

[23] L. M. C. Pereira, U. Wahl, S. Decoster, J. G. Correia, M. R. da Silva, A. Vantomme, and J. P. Araújo, Appl. Phys. Lett. **98**, 201905 (2011).

[24] D. R. Locker and J. M. Meese, IEEE Trans. Nucl. Sci. **19**, 237 (1972).

[25] M. T. Robinson, Phys. Rev. B **40**, 10717 (1989).

[26] S. Zhou, K. Potzger, J. von Borany, R. Grotzschel, W. Skorupa, M. Helm, and J. Fassbender, Phys. Rev. B **77**, 035209 (2008).

[27] U. Wahl, J. G. Correia, S. Cardoso, J. G. Marques, A. Vantomme, and G. Langouche (ISOLDE Collaboration), Nucl. Instrum. Methods Phys. Res., Sect. A **136**, 744 (1998).

[28] U. Wahl, A. Vantomme, G. Langouche, J. P. Araujo, L. Peralta, and J. G. Correia (ISOLDE Collaboration), J. Appl. Phys. **88**, 1319 (2000).

[29] U. Wahl, E. Rita, J. G. Correia, E. Alves, and J. P. Araujo (ISOLDE Collaboration), Appl. Phys. Lett. **82**, 1173 (2003).

[30] A. Janotti and C. G. Van de Walle, Phys. Rev. B **76**, 165202 (2007).

[31] F. Oba, A. Togo, I. Tanaka, J. Paier, and G. Kresse, Phys. Rev. B **77**, 245202 (2008).

[32] F. Oba, M. Choi, A. Togo, A. Seko, and I. Tanaka, J. Phys. Condens. Matter **22**, 384211 (2010).

[33] R. Vidya, P. Ravindran, H. Fjellvag, B. G. Svensson, E. Monakhov, M. Ganchenkova, and R. M. Nieminen, Phys. Rev. B **83**, 045206 (2011).

[34] T. Dietl, H. Ohno, F. Matsukura, J. Cibert, and D. Ferrand, Science **287**, 1019 (2000).

[35] T. Jungwirth, K. Y. Wang, J. Masek, K. W. Edmonds, J. Konig, J. Sinova, M. Polini, N. A. Goncharuk, A. H. MacDonald, M. Sawicki, A. W. Rushforth, R. P. Campion, L. X. Zhao, C. T. Foxon, and B. L. Gallagher, Phys. Rev. B **72**, 165204 (2005).

[36] E. Sarigiannidou, F. Wilhelm, E. Monroy, R. M. Galera, E. Bellet-Amalric, A. Rogalev, J. Goulon, J. Cibert, and H. Mariette, Phys. Rev. B **74**, 041306 (2006).

[37] S. Granville, B. J. Ruck, F. Budde, H. J. Trodahl, and G. V. M. Williams, Phys. Rev. B **81**, 184425 (2010).